10. TUMBLING DRUM PERFORMANCE

The tumbling drums demonstrated at the Quakake site used water power to tumble the stone load inside the drum and cause a grinding action that abrades the limestone surfaces. The limestone fines are then washed from the drum and are dissolved in the neutralization of the acid water. The neutralization performance is dependent on the grinding efficiency of the drums relative to the hydraulic power input of the water. Pearson (3) analyzed the operating characteristics of Zurbuch's drums and presented design procedures which were used to develop the Quakake drums.

Hydraulic Design: Two considerations govern the hydraulic design of the units. First, the turning moment exerted by the water must exceed the resisting moment required to tumble the stone in the drum. Second, the hydraulic efficiency of the drum, which is the ratio between the energy required to tumble the stone to the hydraulic power input, should be maximized.

As shown in Figure 10.1, the turning moment is provided by the weight of water retained by the water wheel blades creating a moment about the center of the drum.

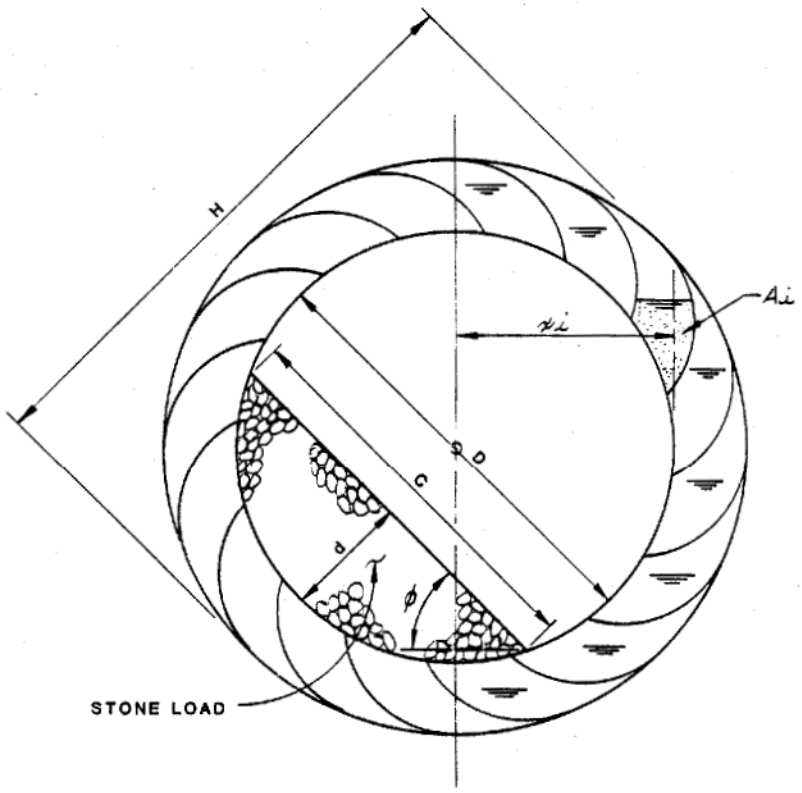

Figure 10.1 Definition Sketch for Analysis of Tumbling Drum

$$M = \sum_{i=1}^{n/2} A_i x_i L \gamma_w \qquad (10.1)$$

Where:

M	=	turning moment, lb-ft.;
n	=	number of vanes
A_i	=	area of water retained by vane i, ft^2;
x_i	=	horizontal distance from the centroid of A_i, ft. to the axis of the drum;
L	=	length of drum, ft.; and,
γ_w	=	unit weight of water, lb/ft^3

An expression for the hydraulic efficiency of the water wheel can be obtained by equating the power available to be used to the power actually used.

$$P_I = \varepsilon Q \gamma_w H \qquad (10.2)$$

Where:

P_I	=	Power supplied, lb-ft/sec.;
H	=	fall of water - outside wheel diameter;
ε	=	efficiency;
Q	=	flow in cfs;

and:

$$P_o = \omega M' = \frac{2\pi N}{60} M' \qquad (10.3)$$

Where:

P_o	=	power consumed; lb-ft/sec.;
ω	=	angular velocity, $sec.^{-1}$;
N	=	$60\ \omega/2\ \pi$, r.p.m.
M'	=	resisting moment ft-lb

When acceleration of the wheel is equal to zero, the turning moment must equal the resisting moment and the flow of water through the wheel equals the product of the maximum volume of the water retained in the buckets formed by adjacent vanes of the water wheel and the number of vanes per second passing a fixed point. Therefore:

$$Q = A_1 L N n/60 \qquad (10.4)$$

Where; A_1 = maximum area, ft^2

Consequently, an expression for hydraulic efficiency can be obtained in which efficiency is expressed as:

$$\varepsilon_h = \frac{P_o}{P_I} = 2\pi \sum_{i=1}^{n/2} A_i X_i /(A_1 n H) \qquad (10.5)$$

Hydraulic efficiency in terms of turning moment becomes:

$$\varepsilon_h = \frac{2\ \pi M'}{A_1 L N \gamma_w H} \qquad (10.6)$$

The turning moment and hydraulic efficiency are functions of the ratio of flow to the rotational speed. For a given maximum bucket area, the ratio between flow and RPM is consistent, as derived by Equation 10.4. For steady flow conditions, an increase in RPM will cause an individual bucket to retain less flow, thereby reducing the available turning moment.

The relationship between Flow/RPM, turning moment and maximum bucket areas for the drum configuration used at Quakake is shown in Figure 10.2. The Flow/RPM ratio causes a change in the hydraulic geometry. Therefore, the hydraulic efficiency of the wheel is altered as shown in Figure 10.2.

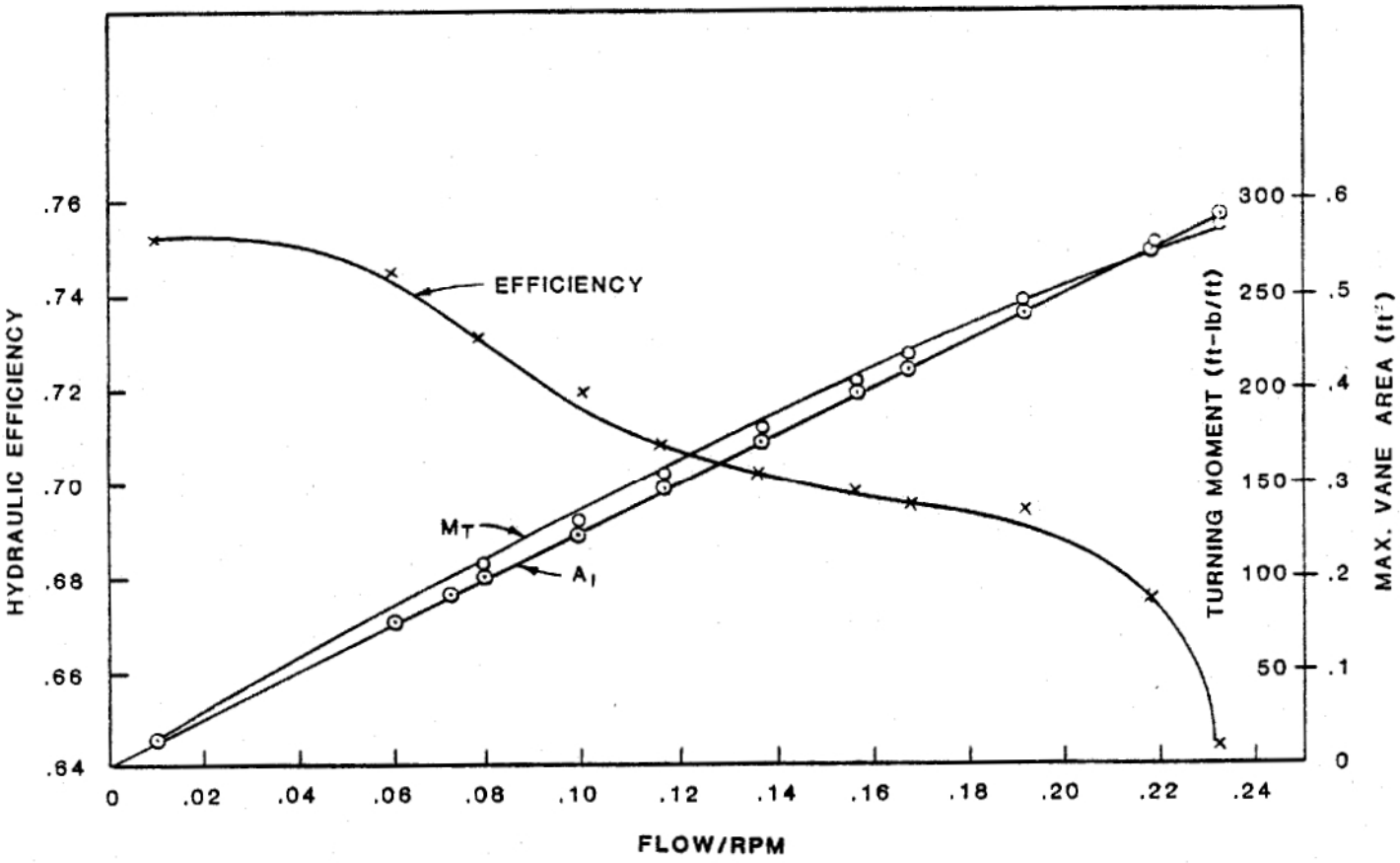

Figure 10.2 Change in Hydraulic Efficiency W/Flow and Rotational Velocity

In addition to the geometric configuration of the drum, factors such as mechanical efficiency and splashing of water from the vanes further reduce the overall efficiency of the wheel. An absorption dynanometer (the Prony Brake shown in Figure 10.3) was used to measure the power output of the drum in the field under actual operating conditions. The Prony Brake consists of two blocks of wood which are forced against the rotating axle thereby absorbing the power of the wheel through friction. A counterbalance using weights and a Lever arm is applied to bring the system into equilibrium and since the torque on the axle and the speed of rotation is known, the

power absorbed by the friction can be computed. When the lever arm is at equilibrium:

$$WL = Fr \qquad (10.7)$$

Where: W = Counter Weight;
L = Lever Arm;
r = Radius of Axle;
F = Effective Force at the Periphery of the Axle.

Since power equals the product of force and distance, divided by the time the force was applied:

$$P = \frac{Fs}{t} = \frac{WL}{r}\frac{s}{t} \qquad (10.8)$$

Where: s = Linear Distance;
t = time;
P = Power.

Converting linear distance to angular for t equal to the time the shaft makes one revolution.

$$S = 2\pi r \qquad (10.9)$$

$$t = 60/(RPM) \qquad (10.10)$$

Therefore: $P = 2\pi(RPM)\,WL/60 \qquad (10.11)$

The results of the Prony Brake tests are shown in Figure 10.4, along with derived efficiencies for the drum operation. As can be seen on Figure 10.4, the measured power is nearly a linear function of flow, thus confirming the relationship expressed by Equation 10.2.

$$P_I = \varepsilon Q \gamma_w H \qquad (10.2)$$

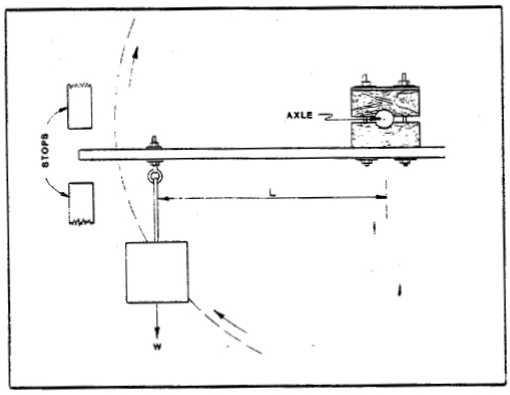

Figure 10.3 Prony Brake Schematic

$$\varepsilon = \varepsilon_h \varepsilon_f \qquad (10.12)$$

Where: ε = Total Efficiency;
ε_h = Hydraulic Efficiency;
ε_f = Mechanical Efficiency

The total drum efficiency is described as the product of the hydraulic efficiency (as previously defined) and the mechanical efficiency. The term "mechanical efficiency" includes the loss of power through splashing in addition to mechanical losses such as bearing friction. For the tests indicated in Figure 10.4, the hydraulic efficiency was 74% and the mechanical efficiency was 80% to 85% within the normal operating range of the drums. An overall efficiency range of 60% to 64% was obtained and allows a determination of the power that can be obtained from the drum to be made in terms of its geometry and supplied flow.

The power consumed by the drum is defined by equation (10.3),

$$P_o = \frac{2 \pi n M'}{60} \qquad (10.3)$$

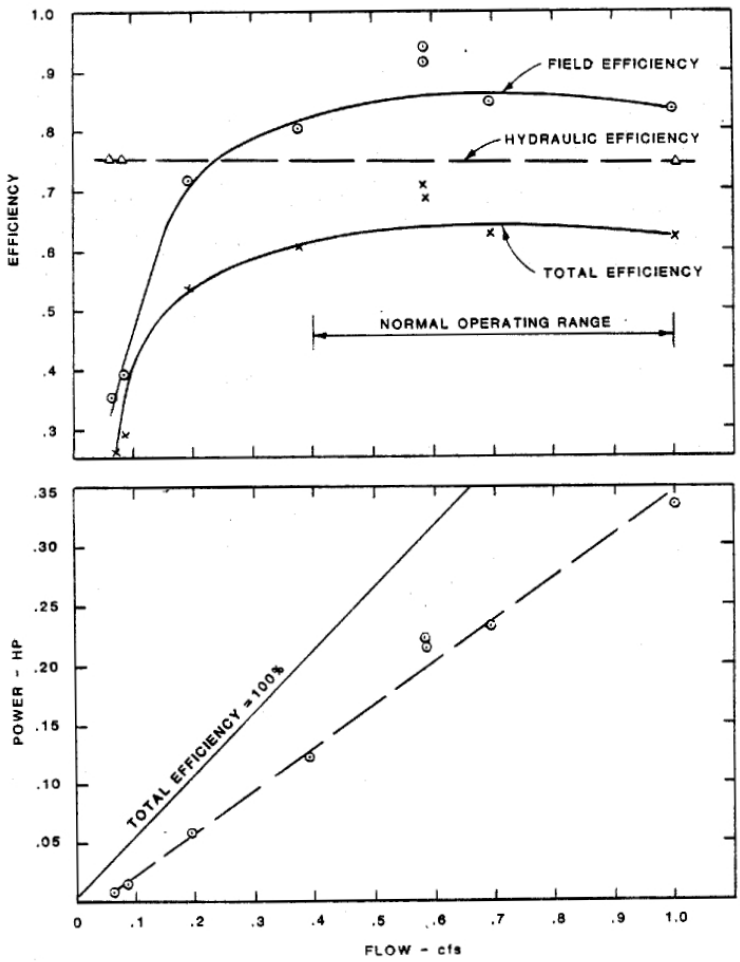

Figure 10.4 Results of Dynamometer Field Testing

and is the power required to maintain the stone load within the drum at a constant angle ~ (See Figure 10.1). This angle is assumed to be similar to the angle of internal friction, or the angle of repose for the crushed limestone used in the drums. The resisting moment is taken as the first moment of the unit weight of stone times the cross section of the stone about the axis of the drum or:

$$M' = \gamma_S C^3 \sin\phi \; L/12 \qquad (10.13)$$

Where:

M'	=	resisting moment in ft-lbs;
γ_S	=	unit weight of stone in lbs/ft^3;
ϕ	=	angle of repose in degrees;
L	=	drum width in ft.;
C	=	chord length of the top of the stone bed in ft. = $2\,(dD-d^2)^{0.5}$
d	=	depth of stone in the drum in ft.;
D	=	diameter of the drum in ft.

Turning moments versus resisting moments, both computed from field measurements, are compared in Figure 10.5. The stones angle of internal friction is shown as variable as it can be expected to change as the stone is ground from an angular shape to a smoothly rounded one. Figure 10.5 indicates a reasonable agreement between theoretical development and the measured data, particularly since a reasonable amount of the scatter can be attributed to measurement accuracy. In addition, the amount of water inside the drum at any particular moment could not be determined in the field. This additional and varying weight of water may have a significant effect on the actual resisting moment. The actual and theoretical values are also compared in Figure 10.6 by plotting the stone load in the drum against the ratio of flow to RPM.

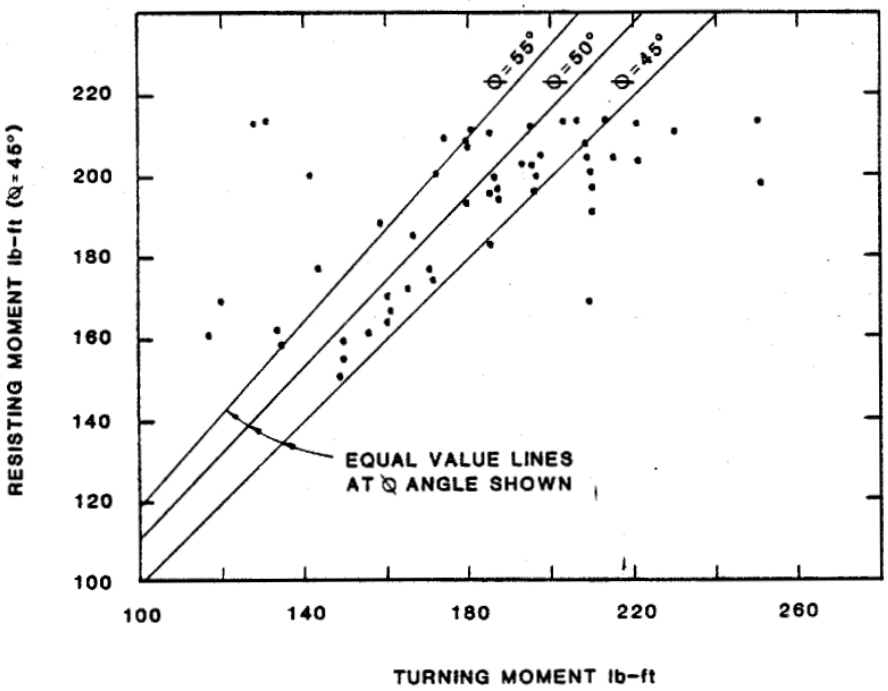

Figure 10.5 Turning Moment Resisting Moment Comparison

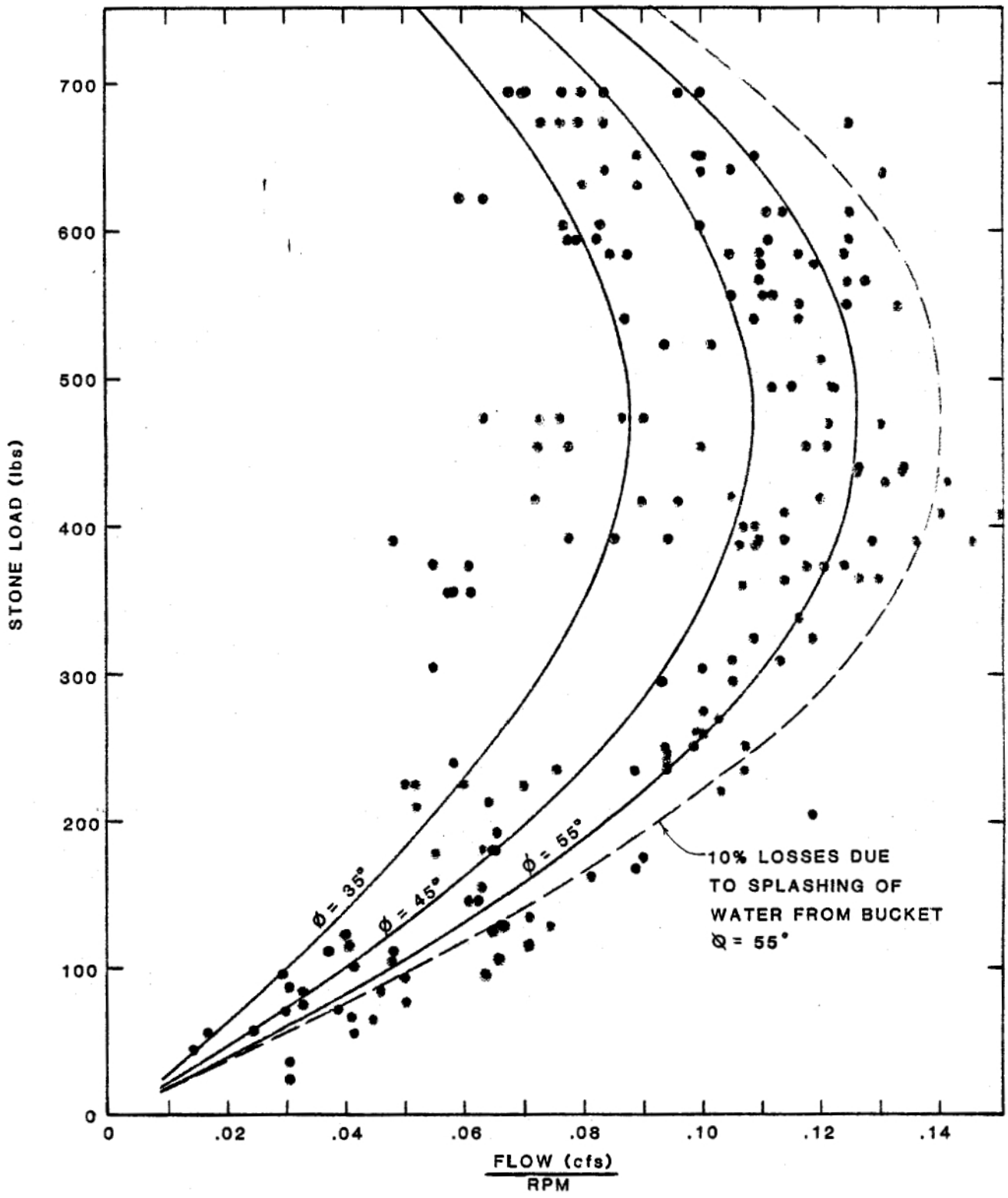

Figure 10.6 Measures of Stone Load - Flow/RPH Relationships

The configuration of the flume or pipe which delivers the water to the wheel affects the drums performance significantly. The differences in total efficiency caused by varying inlet configurations are presented in Figure 10.7. The water should be delivered to the wheel as smoothly as practical with a minimum of splashing so that maximum wheel efficiency can be achieved. In addition, the hydraulics of the outlet conveying water away from the drum requires adequate sizing. If water is allowed to cover even a small portion of the wheel, the drums performance is severely curtailed due to the additional drag created by the submergence.

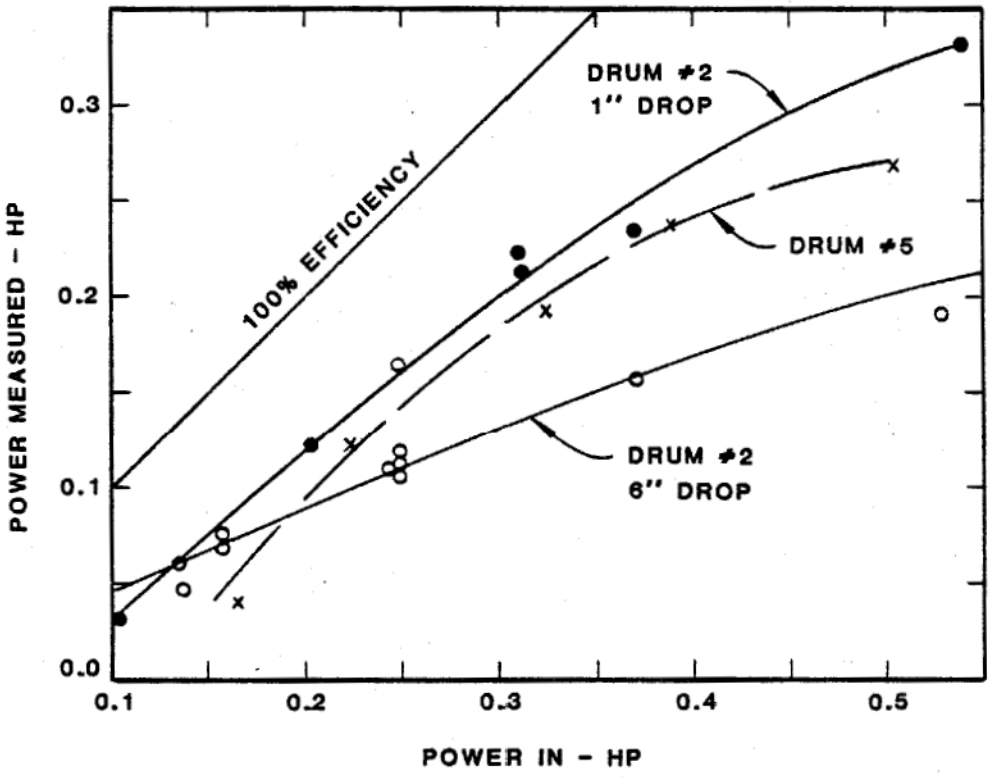

Figure 10.7 Change in Output Power with Flume Geometry

Limestone Fines Production: The production rate of fines, in pounds per hour was determined from field measurements of limestone load depletion in drums, at various intervals. Relationship between production rate, flow rate and drum rotation is presented in Figure 10.8 and indicates that although fines production cannot be directly correlated with the flow rate, an increase in production rate is associated with an increase in rotation rate. The increase in fines production with increasing RPM is directly related to the level of stone in the drum as shown in Figure 10.9. There appears to be several reasons for the observed variations in fines production, independent of the measured parameters. First, the rate of production of fines was much higher for fresh angular stone (12 to 24 lb/hr) than for stone that had become abraded to an egglike shape (similar to river pebbles (2 to 6 lb/hr). Consequently, the degree and rate of stone rounding appear to be important design parameters which require additional evaluation. Second, the methods employed for the determination of the limestone load depletion in the drums were not accurate enough to evaluate the relatively minor changes in load over short time intervals. A drum weighing mechanism consisting of a hydraulic cylinder and pressure gage had been incorporated into the design of the facility. However, its maximum accuracy was limited to 25+ pounds and could not reliably measure hourly changes in stone weight. A weight and lever arm system was used in Run No. 4 with improved results. The majority of the measurements, however, were determined by correlating the pressure cell reading with volumetric measurements of the stone in the drum. Third, the observed increase in fines production at high RPM's and stone loads less than 35% of the drum capacity probably represents a fundamental change in the assumed mechanics of the abrasion process itself. At this point, the fines production becomes more dependent on the speed of rotation of the drums.

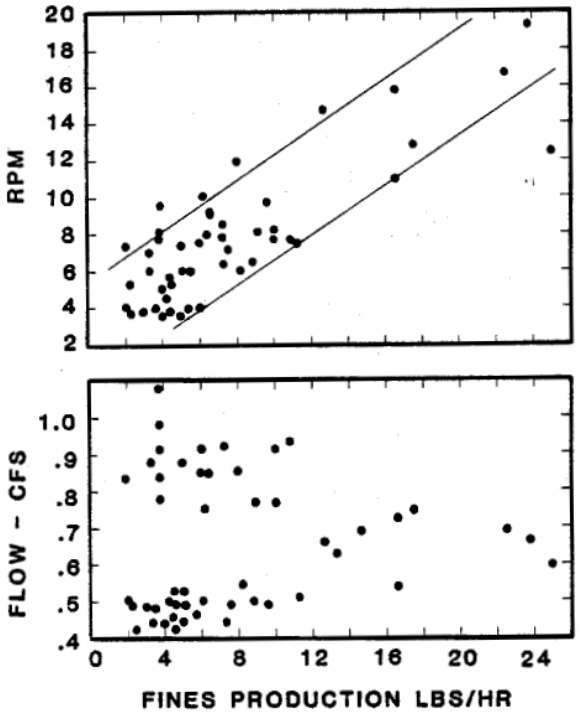

Figure 10.8 Limestone Fines Production Compared to Flow & RPM

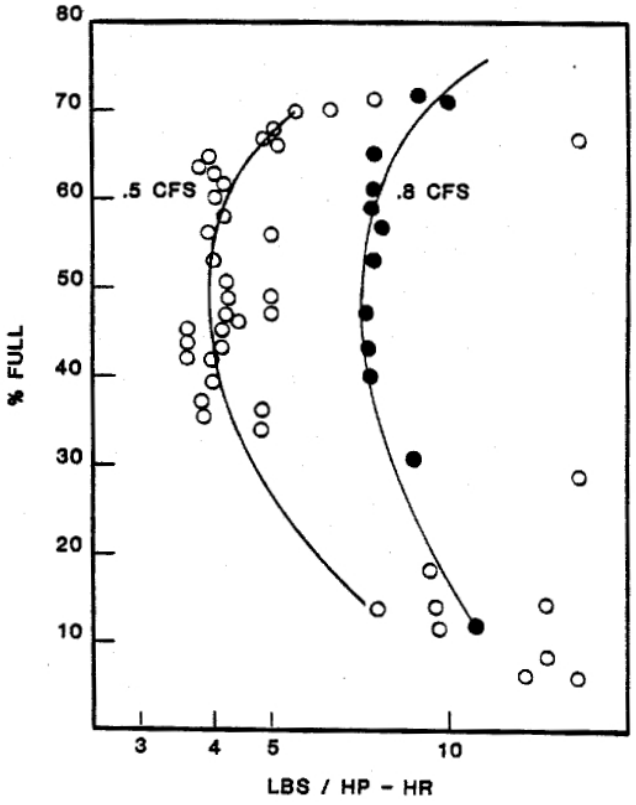

Figure 10.9 Limestone Fines Production Compared to Flow & Stone Load

Fortunately, these sources of variation in individual measurements of the fines production rate are not persistent over the long term operation of the drums. Therefore, average rates of fines production determined from these data, provide a reliable measure for this aspect of process characteristics. The cumulative loss of weight of the limestone versus cumulative hydraulic energy expended in the drums is presented in Figure 10.10.

The average rate of fines production was 41.4 pounds of limestone per horsepower per hour for drums starting at 70% of their capacity and operating until the stone is depleted. However, the production rate is not evenly distributed. When the effects of the fresh angular stone and the high RPM's at low stone weights are not considered, the average production rate drops to 26.5 lbs/HP-HR. This rate appears to be very consistent in the operating range where the drum is 65% to 36% full.

Production rates as high as 55 lbs/HP-HR were observed for the angular stone in freshly filled drums. For the case where stone loads were maintained below 35% full, the average production rate was greater than 90 lbs/HP-HR, suggesting that this would be the optimum operating range if the attendant stone feeding problems could be resolved.

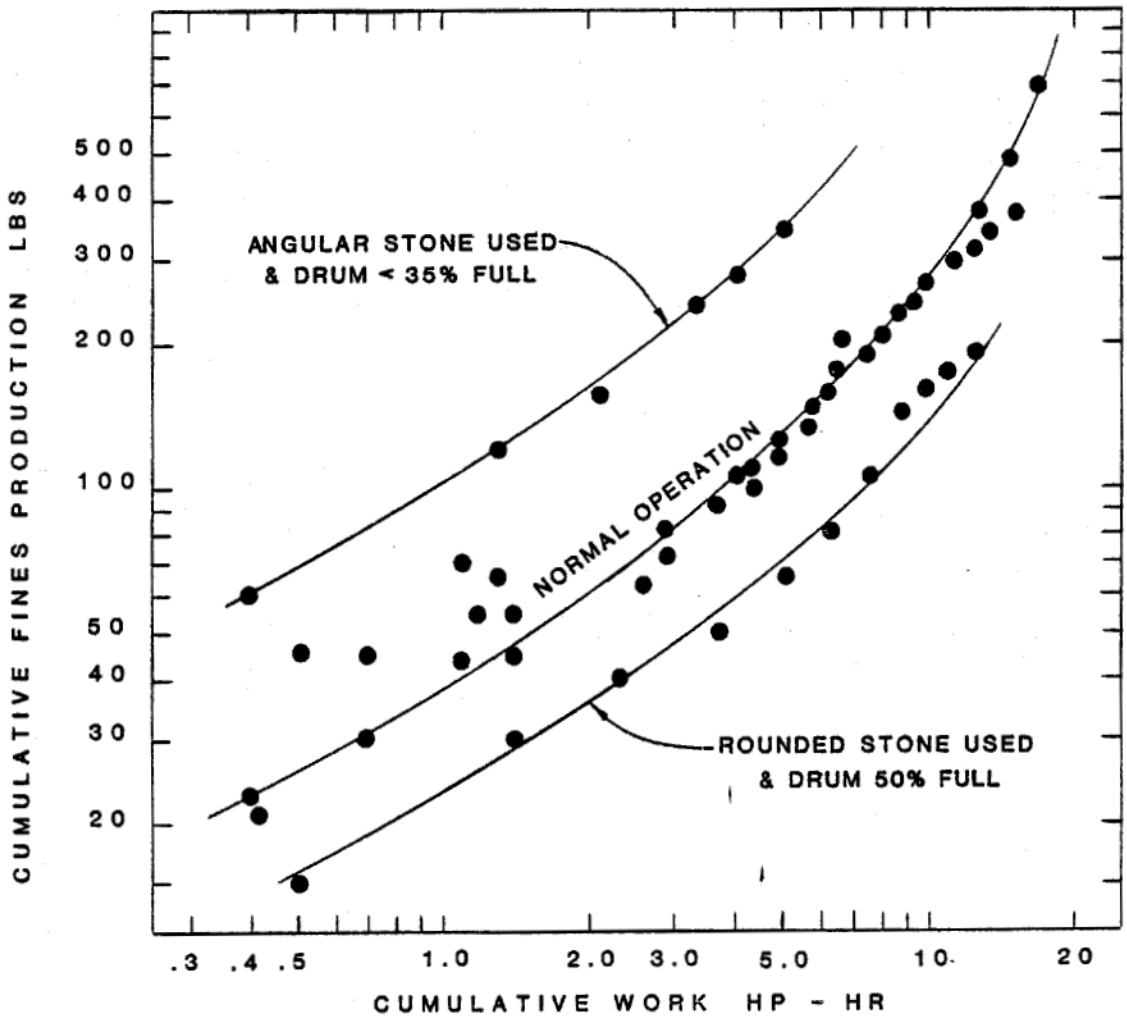

Figure 10.10 Limestone Fines Production Compared to Cummulative Work

Treatment Results: As mentioned, of the five tumbling drums installed at Quakake, three were placed in series to perform a complete treatment unit. The following discussion pertains primarily to this process unit. Complete testing results and field operating data are presented in Appendix "C".

The overall performance of the drum treatment process is illustrated in Figure 10..11. Fines production in terms of pounds per hour per cfs of AMD flow is plotted against pH values achieved at the end of the process (final pH). The points labled ultimate pH represent the pH values achieved through detention and aeration of the process effluent. Despite the data scatter, Figure 10.11 provides a reasonable illustration of the overall process performance. However, an accurate evaluation of the drums performance based on an instantaneous rate of fines production is not practical for the following reasons. First, all the fines introduced into the system do not dissolve immediately. The neutralization is provided by limestone fines trapped in the drum bays, as well as the amount of fines being introduced at any given time. This is illustrated by the fact that pH values as high as 5.5 were observed in the process effluent after the drums had been running empty for several hours. The second factor affecting evaluation of the results is the difficulty in obtaining accurate instantaneous measurements of the limestone dissolution and carbon dioxide exsolution processes, which are very time dependent. Small changes in the process system or in sample handling and testing methods can cause significant change in the observed results.

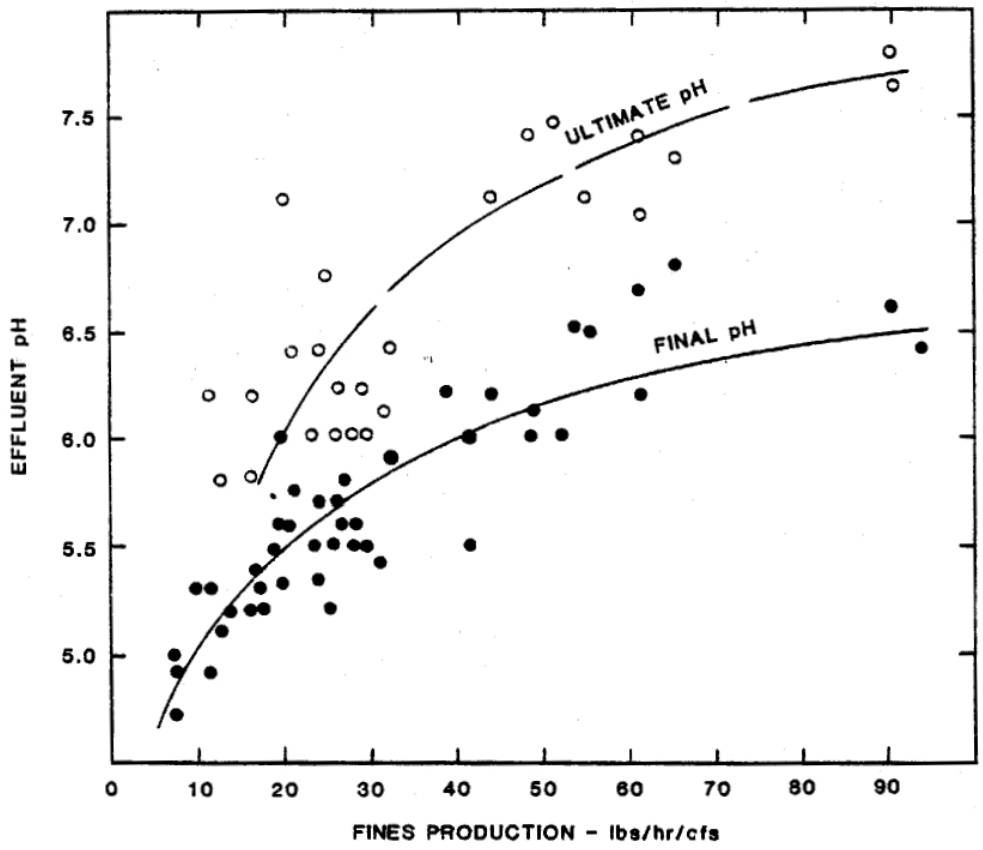

Figure 10.11 Effluent pH Compared to Limestone Fines Production Final pH values are measurements prior to detention and aeration. Ultimate pH values are for measurements after aeration.

Efficiency of the process, expressed by comparing limestone fines production with the acid neutralized and with the alkalinity introduced into the system, is shown on Figure 10.12. It should be noted that efficiencies in terms of alkalinity shown on Figure 10.12 are based on alkalinity determinations made to a fixed end point of pH 4.5. Whereas, the titration curves obtained during Run No. 4 indicate that the actual endpoint value should be closer to a pH of 5.2.

The close spacing of the drum units resulted in the AMD having a very short travel time (25 to 30 seconds) through the process. Consequently, a large amount of fines were washed through the system without having time to fully react with the acid water. This is illustrated in Figure 10.13 where the efficiency of the acidity reduction is plotted against the production of fines. The figure shows that the process is most efficient at lower limestone fines production rates, where the fines had sufficient time to react with the AMD. The dissolution of the limestone particles (and therefore the neutralization process) is dependent on time and pH. For example, the alkalinity increase resulting from limestone dissolution can be formulated as:

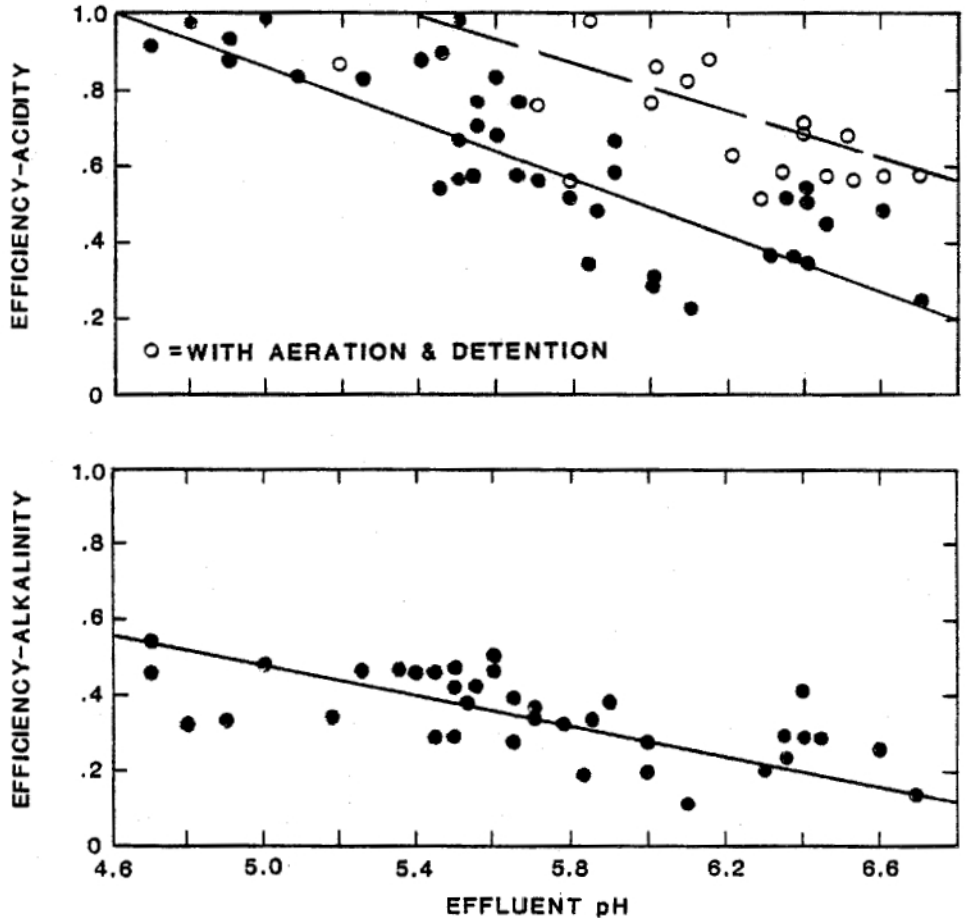

Figure 10.12 Acidity and Alkalinity Use Efficiencies at Various Effluent pH Values. Note that aeration and detention increased the process efficiency almost by a factor of 3.

$$[ALK] = \frac{2w}{v} = \frac{2\gamma\delta\alpha Q}{v} = \frac{2\gamma\delta\alpha v}{vt} = \frac{2\gamma\delta\alpha}{t} \qquad (10.14)$$

in which:

w	=	mass of limestone dissolved, kg mole
v	=	volume of AMD, m^3
γ	=	molar density of limestone, kg mole $-m^{-3}$
δ	=	thickness of limestone film dissolved, m
α	=	surface area of limestone particle, m^2
Q	=	AMD flow rate, m^3 sec^{-1}
t	=	Contact time between limestone and AMD, sec.

The rate of decrease of the diameter of a particle can be obtained by differentiating Eq. 10.14 and combining it with Eq. 4.4:

$$\frac{\delta}{t} = \frac{d[ALK]}{\gamma d\alpha} = 2\frac{k_1[H+]}{\gamma} \qquad (10.15)$$

Then for k_1 = 0.0055 m - sec^{-1}
γ = 27 kg mole - m^3;

At a pH of 3.0, the time required to dissolve a 0.1 mm diameter limestone particle is 2 minutes. Whereas, 3.4 hours are required to dissolve the same size particle when the pH of the AMD is equal to 5.0.

In order to increase the efficiency of the drum neutralization process, it is necessary to match the production rate to the particle dissolution rate within practical limits. In addition, the limestone particles should be kept in suspension while they dissolve in order to realize the full neutralization potential of the limestone. Particles which have settled to a stream bed become less effective for the neutralization purposes. The desired equilibrium between production and dissolution can be obtained by detention between drum units and by reducing the particle sizes being discharged from a drum. The effect of the small detention pond provided during the fourth run is shown in Figure 10.14 and shows that even a small amount of detention (less than 10 min.) has a beneficial effect on the efficiency of the system. Had the pond been placed between the first and second drums rather than between the second and third, the increase in efficiency would have been much higher due to the lower pH of the effluent of the first drum.

Detention and turbulence of the tumbling drum effluent will also enhance the neutralization process by increasing the rate of CO2 exsolution. The carbon dioxide levels observed in the drum process are shown on Figure 10.15. The values given should not be construed as actual CO2 values as they are an approximation of the true value derived from 'the difference of the "hot" and "cold" acidity titrations. There is no direct, simple method to titrate directly for individual values of H2CO3. The values given do reflect the relative change of CO2 throughout the process and can be used to evaluate the effects of this change. The CO2 values plotted on Figure 10.15 are mean values for Run No. 4. The individual values varied considerably and the ranges of observed results are also indicated in Figure 10.15.

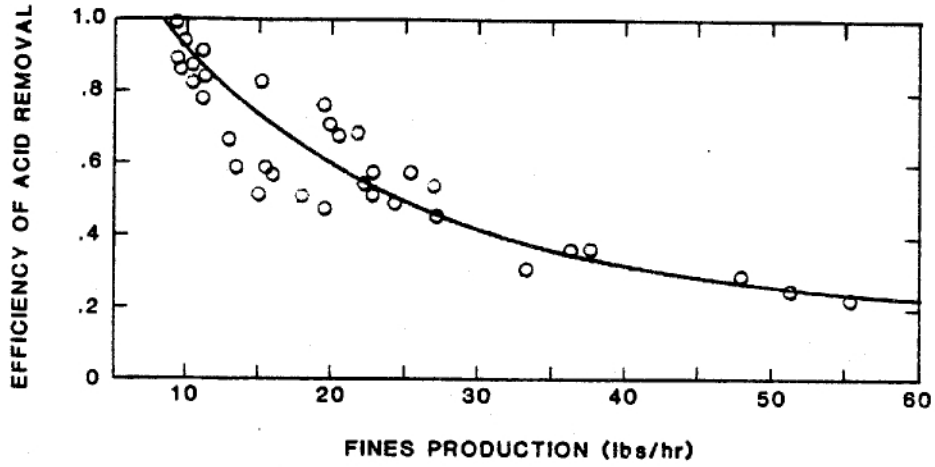

Figure 10.13 Acid Removal Efficiency Compared to Limestone Fines Production. Aerated efficiencies not shown.

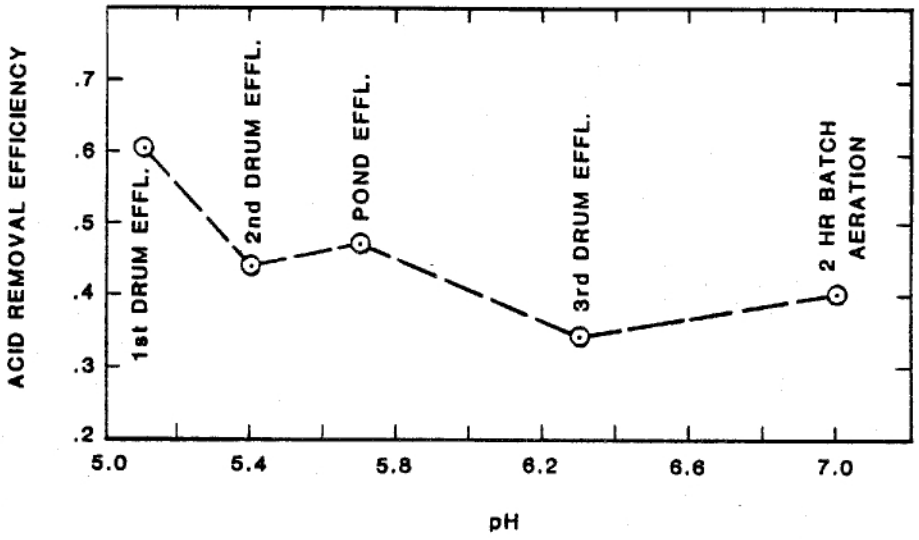

Figure 10.14 Acid Removal Efficiency for an Average Drum Run

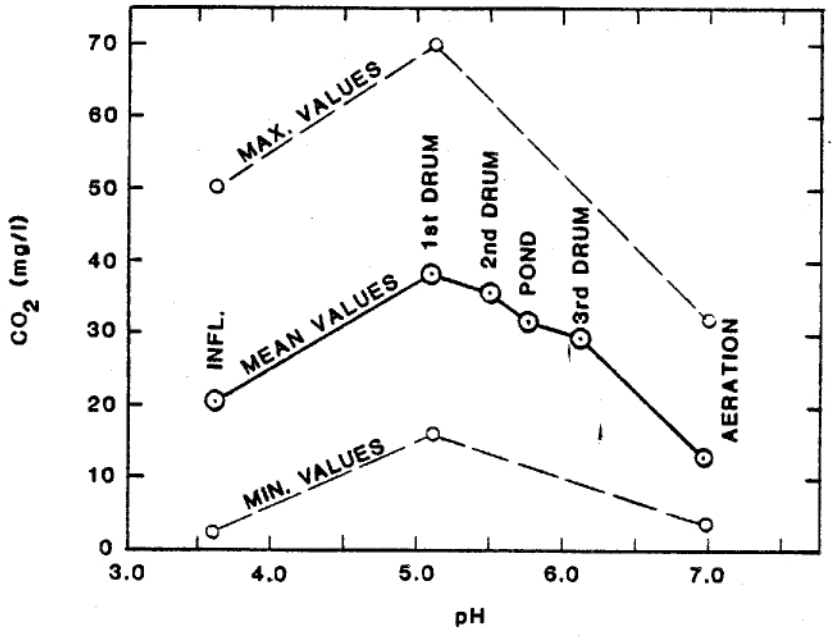

Figure 10.15 Average Carbon Dioxide Concentration for a Typical Drum Run

Aeration: During Run No. 4, facilities were provided to perform carbon dioxide stripping tests by aeration of the tumbling drum effluent. Batch CO2 stripping tests were performed in a 500 gallon tank with air supplied from a compressor unit through 2 porous stone diffusers. The mean results of these batch tests are shown in Figure 10.15.

The theoretical aspects for the decarbonation of limestone-neutralized AMD has been presented by Pearson (24) and demonstrated in the laboratory using the apparatus shown in Figure 10.16. The laboratory tests were performed on distilled water to which sodium carbonate was added. Tests were performed in the field using similar equipment in order to confirm that conclusions drawn from the lab tests were applicable to the stripping of CO2 from AMD. The field column tests were performed on the effluent from the downflow units which had a pH of 5.6 prior to aeration. The results of the two column tests are shown on Figure 10.17 and indicate good agreement. Results of the batch aeration tests of the tumbling drum effluent are also superimposed on this Figure. A direct comparison of results in other than general terms is not possible as the results of batch tests indicate a continuing reaction with suspended limestone particles. The results confirm the applicability of Pearson's procedures as a valid design method for determining the effects of aeration on limestone neutralized AMD.

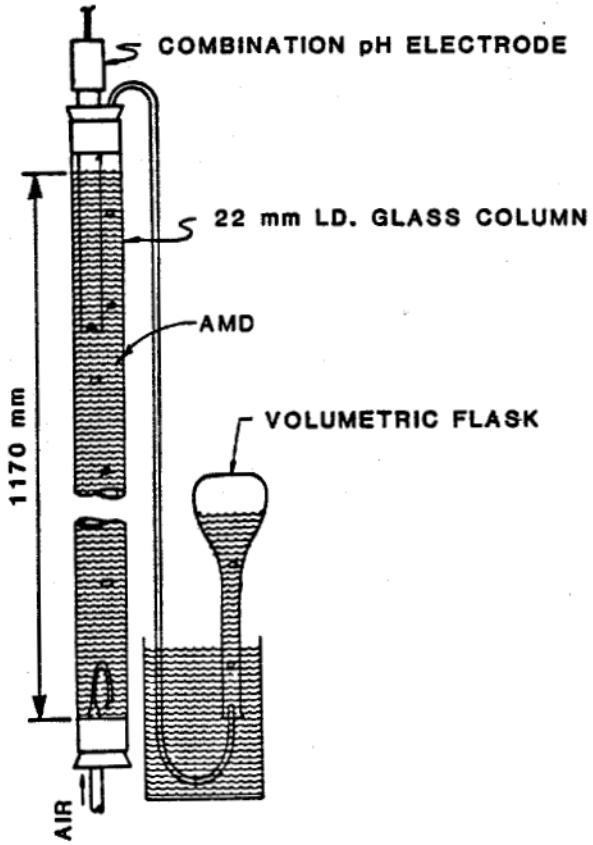

Figure 10.16 Decarbonation Test Apparatus

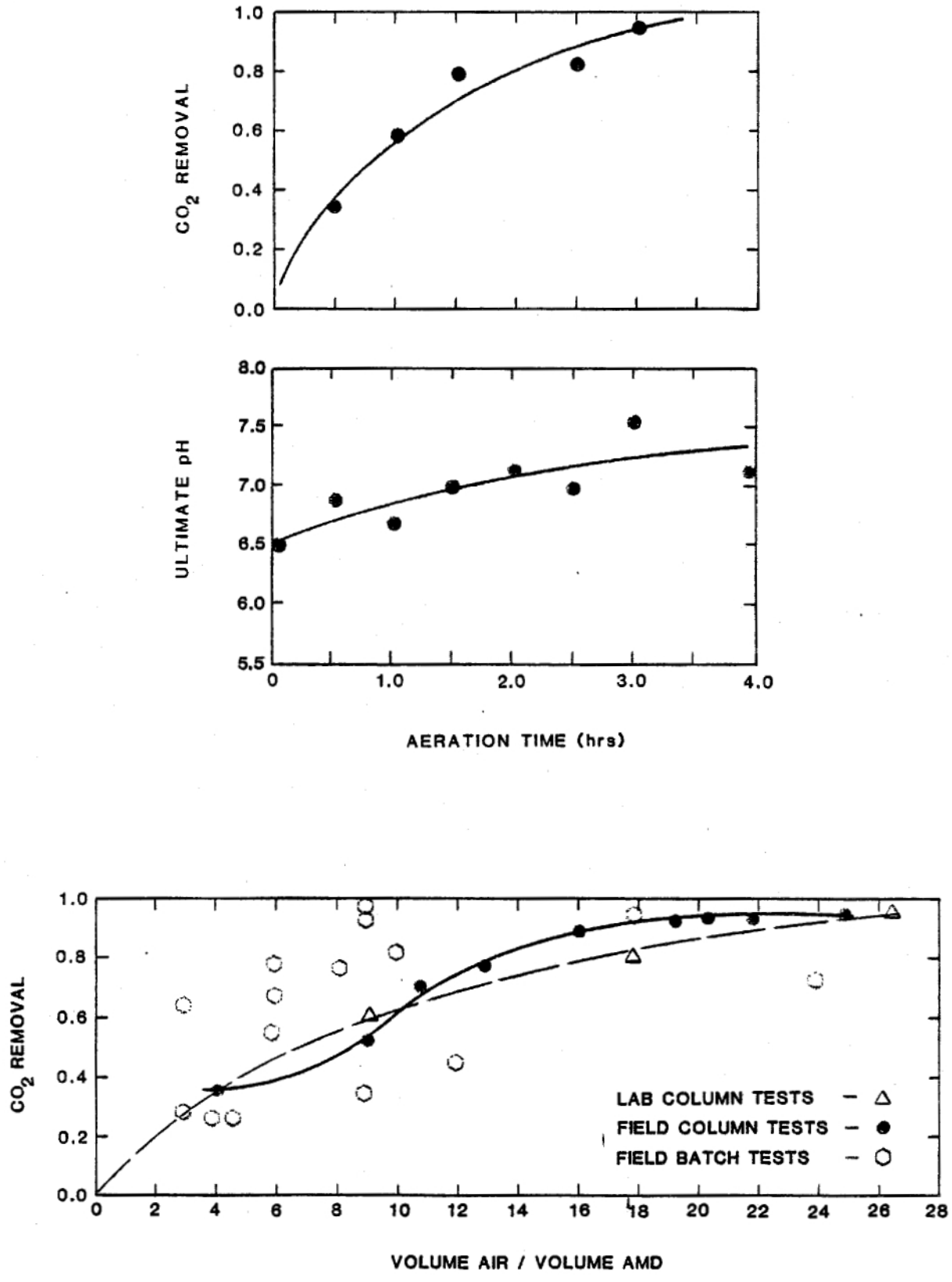

Figure 10.17 Aeration Effort Compared with CO_2 Removal and Effluent pH